Force on spindle microtubule minus ends moves chromosomes

Mary Williard Elting,[1] Christina L. Hueschen,[1,2] Dylan B. Udy,[1] and Sophie Dumont[1,2,3]

[1]Department of Cell and Tissue Biology, [2]Biomedical Sciences Graduate Program, and [3]Department of Cellular and Molecular Pharmacology, University of California, San Francisco, San Francisco, CA 94143

The spindle is a dynamic self-assembling machine that coordinates mitosis. The spindle's function depends on its ability to organize microtubules into poles and maintain pole structure despite mechanical challenges and component turnover. Although we know that dynein and NuMA mediate pole formation, our understanding of the forces dynamically maintaining poles is limited: we do not know where and how quickly they act or their strength and structural impact. Using laser ablation to cut spindle microtubules, we identify a force that rapidly and robustly pulls severed microtubules and chromosomes poleward, overpowering opposing forces and repairing spindle architecture. Molecular imaging and biophysical analysis suggest that transport is powered by dynein pulling on minus ends of severed microtubules. NuMA and dynein/dynactin are specifically enriched at new minus ends within seconds, reanchoring minus ends to the spindle and delivering them to poles. This force on minus ends represents a newly uncovered chromosome transport mechanism that is independent of plus end forces at kinetochores and is well suited to robustly maintain spindle mechanical integrity.

Introduction

During cell division, the mitotic spindle assembles itself from its constituent parts. Spindle microtubule minus ends are focused into two poles, and these poles dictate where duplicated chromatids are transported at anaphase. Forces that focus microtubules into poles are crucial to spindle organization and function. Cytoplasmic dynein, a minus end–directed microtubule motor, clusters parallel microtubules into spindle poles (Verde et al., 1991; Heald et al., 1996) and transports the microtubule-binding protein NuMA to build poles (Merdes et al., 2000). At poles, dynein and NuMA tether microtubules (Gaglio et al., 1995; Merdes et al., 1996; Heald et al., 1997; Dionne et al., 1999), and pole structure remains robust despite rapid microtubule turnover (Saxton et al., 1984) and opposing tension on kinetochore fibers (k-fibers) from kinetochore-based forces (Gordon et al., 2001; Manning and Compton, 2007; Silk et al., 2009). Thus, poles must both oppose force and be constantly rebuilt (Gaglio et al., 1997; Goshima et al., 2005). This engineering challenge highlights a long-standing paradox: how can the spindle maintain its structure and mechanical integrity and yet remain dynamic, flexible, and architecturally plastic, as its functions require?

For the spindle to preserve its structural integrity, it must be able to continuously rebuild poles by recognizing and sorting new microtubule structures. Indeed, during spindle assembly, poles can integrate both new peripheral microtubules (Rusan et al., 2002; Tulu et al., 2003) and kinetochore-nucleated k-fibers (Khodjakov et al., 2003; Maiato et al., 2004). Established spindles can move short microtubule seeds to poles (Heald et al., 1996, 1997) and reincorporate k-fibers severed by ablation as microtubules grow back (Snyder et al., 1991; Chen and Zhang, 2004; Maiato et al., 2004), and poles from different spindles can fuse together (Gatlin et al., 2009). Although dynein and NuMA are either demonstrated or suspected to mediate these observations of dynamic microtubule integration into poles, it is not clear which microtubule structures serve as dynein cargo, where on them force is exerted, or how strong that force is. We do not know how forces that maintain poles compare to other spindle forces or on what timescale they contribute to spindle architecture. In large part, this is because the response of the established spindle to detached microtubules is challenging to study: k-fiber minus ends are already embedded in the spindle and free microtubules within the spindle body are difficult to image.

M.W. Elting and C.L. Hueschen contributed equally to this paper.
Correspondence to Sophie Dumont: sophie.dumont@ucsf.edu
Abbreviations used in this paper: K-fiber, kinetochore fiber; STLC, S-trityl-ʟ-cysteine.

Figure 1. Microtubule severance triggers a response that rapidly pulls detached microtubules toward spindle poles. (A) To probe forces that maintain spindle poles, we challenge the spindle steady-state by detaching microtubules from poles using laser ablation. (B–F) Time-lapse live images of GFP–α-tubulin PtK2 cells (phase contrast, blue; GFP–α-tubulin, yellow). Time is in min:s, with frame captured immediately after ablation set to 00:00. Bars, 2 µm. Arrowheads mark minus ends of ablated microtubules. Dotted lines indicate the position of the kinetochore end of the ablated k-fiber (B–D and F) or bundle minus end (E) immediately before ablation. (B) Representative response of metaphase spindle to k-fiber laser ablation (marked by X). After ablation, the centromere initially relaxes, causing the ablated k-fiber stub to move upward (00:00–00:08). During this time, the k-fiber stub also rotates freely and the uncapped (and unstable) microtubule plus ends depolymerize. Then, the k-fiber stub is pulled rapidly poleward, stretching the centromere and dragging the attached chromosome poleward (00:08–02:01). Minus ends are reincorporated into the spindle (rightmost panel), and the chromosome then resumes typical metaphase oscillations (not depicted). The kinetochore whose k-fiber is ablated is marked by an asterisk and its sister by an o. See also Video 1. (C) Representative response of anaphase spindle to k-fiber laser ablation (X). After ablation, the k-fiber stub rotates freely and its attached chromatid moves upward (00:00–00:21). Upon apparent contact with a neighboring microtubule (00:21), the k-fiber stub is pulled poleward faster than typical anaphase chromatid movement (times 00:21–01:15). The kinetochore of the ablated k-fiber (*) is pulled rapidly toward the pole, passing a neighboring control chromosome (o). See also Fig. S2 and Video 2. (D) Representative response of monopolar spindle to k-fiber laser ablation (X). Immediately after ablation, the k-fiber stub rotates freely, but its attached chromosome does not move upward, consistent with a lack of force from a sister half-spindle (00:00–00:07). Then, the k-fiber stub is pulled poleward, dragging the attached chromosome by its kinetochore (*; 00:07–00:35). The kinetochore of an unmanipulated neighboring

k-fiber is marked by o. See also Video 3. (E) Representative response of monopolar spindle to non–k-fiber bundle laser ablation (X). Almost immediately after ablation, the severed non–k-fiber bundle is rapidly pulled toward the pole (00:06–00:32). See also Video 4. (F) Representative response of cell to ablation (X) of the newly created microtubule minus end. After a first ablation (00:00), the k-fiber stub (kinetochore marked by asterisk) is pulled poleward (00:00–00:53). A second ablation destroys the k-fiber stub minus end (01:03), and poleward movement temporarily stops (01:03–01:10), suggesting that poleward force generation requires the minus end. A second poleward transport phase follows this pause (01:28–01:46). See also Video 7.
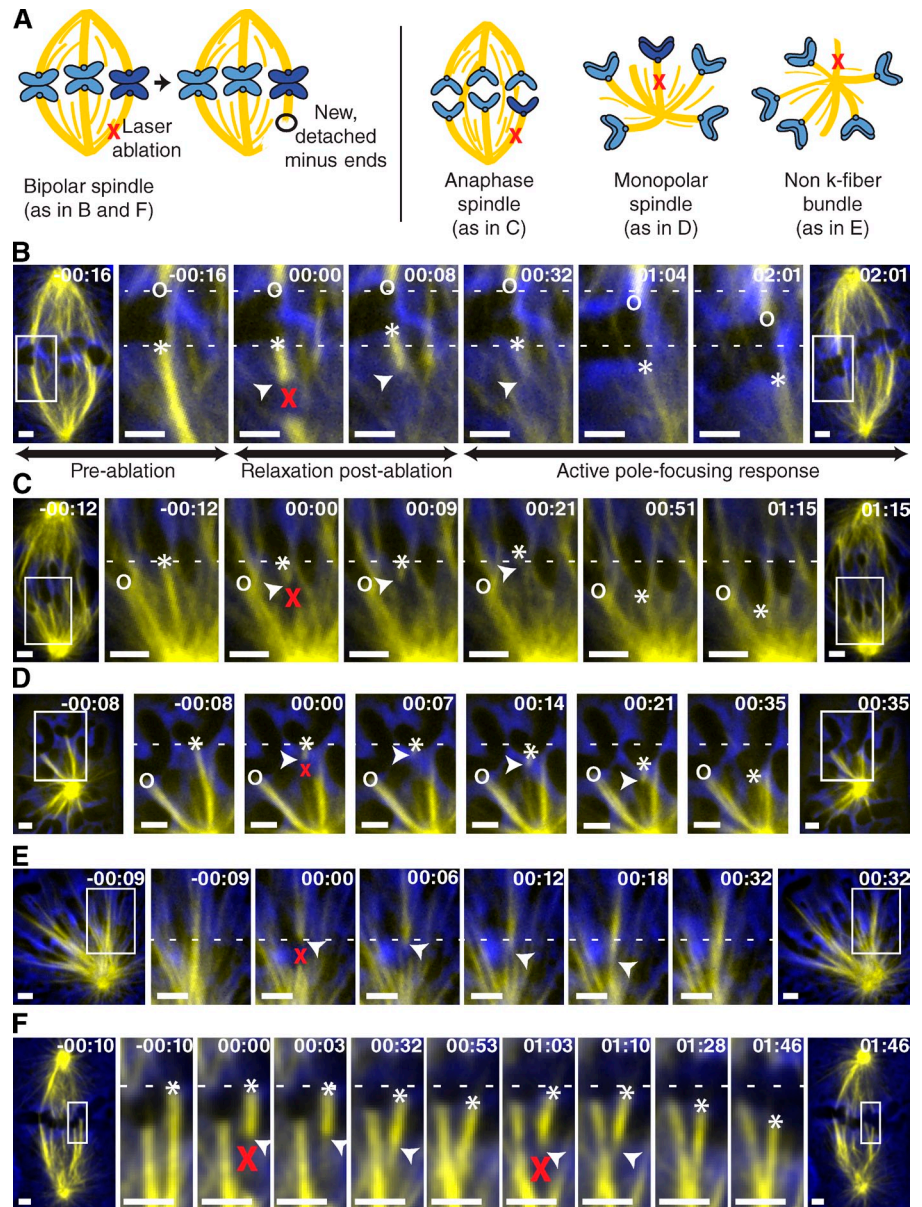
Here, we use laser ablation to challenge the spindle's architectural steady state by detaching microtubules from poles and we probe cellular forces exerted on, and molecules recruited to, these microtubules. We show that detached microtubules are rapidly identified by dynein/dynactin and NuMA and transported toward poles, overpowering opposing forces on microtubules and chromosomes to repair spindle architecture. Force is generated by localized pulling on new minus ends, which powers a newly identified mechanism of chromosome movement at mitosis, independent of kinetochore forces. We propose that rapid detection and dominant poleward transport of free minus ends by dynein maintains spindle integrity throughout mitosis, making k-fiber anchorage and spindle pole structure robust to component turnover and mechanical challenges.

Results

K-fiber severance triggers poleward chromosome movement within seconds

We used pulsed laser ablation to sever microtubules and detach them from poles (Fig. 1 A) in mammalian GFP–α-tubulin PtK2 cells. In metaphase spindles, we ablated k-fibers a mean distance of 2.5 ± 0.1 µm from the kinetochore, leaving a short k-fiber "stub" that terminated with new microtubule minus ends. In the brief first response phase after ablation, the previously stretched centromere rapidly relaxed, causing the k-fiber stub to move toward the chromosome, and the uncapped (and unstable) microtubule plus ends created by k-fiber severance quickly depolymerized (Spurck et al., 1990; Maiato et al., 2004; Brugués
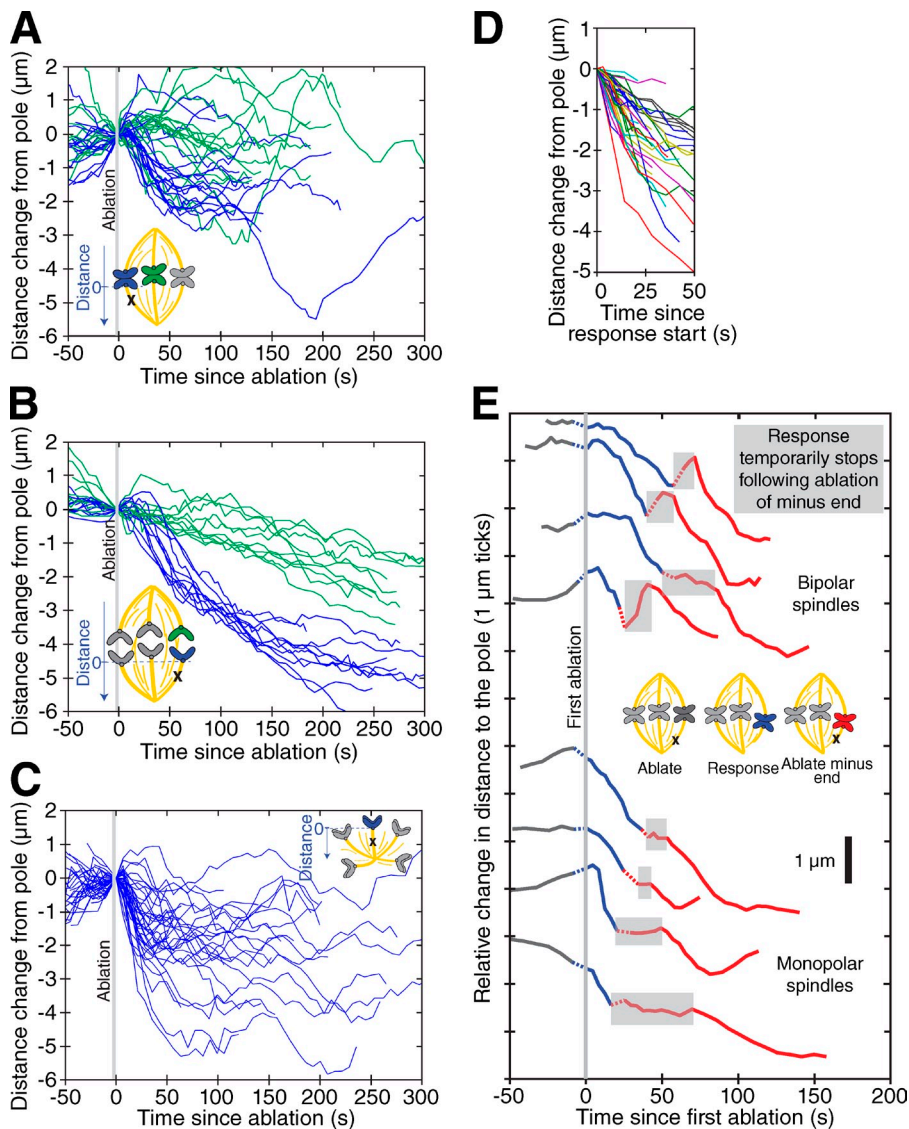
Figure 2. **Dynamics of the poleward transport response suggest it acts rapidly and moves chromosomes robustly across different spindle architectures.** (A) Change in the distance from chromosomes to the pole before and after ablation of their k-fibers in metaphase bipolar spindles. After ablation, chromosomes attached to ablated k-fibers (blue traces, $n = 18$) are pulled poleward, whereas neighboring control chromosomes (green traces, $n = 14$) continue oscillating. (B) Change in the distance from chromatids to the pole before and after ablation of their k-fibers during anaphase. Chromatids attached to ablated k-fibers (blue traces, $n = 10$) are pulled toward poles faster than anaphase movement of their unmanipulated sister chromatids (green traces, $n = 10$) before resuming normal anaphase movement around 70 s. See also Fig. S2. (C) Change in the distance from chromosomes to the pole before and after the ablation of their k-fibers in monopolar spindles. After ablation of their k-fibers, chromosomes are rapidly pulled toward poles (blue traces, $n = 37$) before resuming normal oscillations. (D) Zoom of traces from C displaying only from start to end of the poleward transport response of each trace, synchronized to individual response start times (0 s). (E) Change in the distance from chromosomes to the pole during repeated ablation experiments in bipolar (top) and monopolar (bottom) spindles (four example traces of each). Traces are shown in gray before the first ablation, in solid blue after the first ablation (which severs the k-fiber), and in solid red after the second ablation (which destroys the new, free minus ends). Dotted lines connect points before and after ablation. Poleward transport begins after the first ablation but temporarily stops when the k-fiber stub minus end is destroyed by the second ablation, suggesting that poleward transport requires mechanical engagement of the minus end.

et al., 2012; Sheykhani et al., 2013; Fig. 1 B and Video 1). These mechanical cues verified that ablation severed k-fibers (see Materials and methods).

Then, beginning after a mean delay of 15 ± 4 s following ablation, the k-fiber stub was rapidly transported back toward the spindle pole to which it was previously connected, dragging its attached chromosome and stretching the centromere back to preablation levels (Fig. 1 B, Fig. 2 A, Table 1, and Video 1). This poleward transport comprised a distinct, second response phase and was unexpected given the loss of a direct connection of the k-fiber to the pole. The severed k-fiber often began moving before its nonablated sister k-fiber and the centromere stretched rather than compressed during movement, both indicating that movement was powered by pulling forces on the severed k-fiber rather than by pushing forces from the sister. In some cases, the initiation of movement coincided with the k-fiber stub end visibly contacting a neighboring microtubule or k-fiber. Chromosomes moved poleward at a mean speed of 2.2 ± 0.2 µm/min after ablation (Table 1), significantly faster than normal poleward chromosome speeds at metaphase (1.3 ± 0.2 µm/min; Table 1).

Transport persisted for an average of 60 ± 7 s and 2.1 ± 0.1 µm, indicating processive force generation. After each discrete episode of poleward movement in response to ablation, the k-fiber stub was reincorporated into the spindle and chromosomes resumed normal metaphase oscillations. Cells entered anaphase even after numerous ablations. Thus, k-fiber severance reveals that chromosomes can be pulled poleward (and centromeres can be stretched) without direct k-fiber stub connection to the pole, suggesting a force-generating attachment of the stub to the spindle body.

The poleward transport force overpowers other forces on chromosomes and microtubules to move chromosomes

To probe the magnitude of the poleward transport force and its structural impact on the spindle, we compared its poleward pull on chromosomes to other spindle forces, such as opposing tension from a sister k-fiber (Fig. 1 A). We ablated k-fibers during anaphase, when chromatids are no longer strongly attached to their sisters. As at metaphase, k-fiber stubs and attached chromatids

Table 1. Characterization of the poleward transport response in mechanically distinct systems

Experimental condition	Poleward speed	Delay between end of ablation and response	Duration of pole- ward movement	Magnitude of pole- ward movement	Number of ablations (n) and number of cells (x)
	μm/min	s	s	μm	
Metaphase bipole ablation	2.2 ± 0.2	15 ± 4	60 ± 7 (n = 14, x = 13)	2.1 ± 0.1 (n = 14, x = 13)	n = 18, x = 17
Metaphase bipole control	1.3 ± 0.2	56 ± 11[a]	64 ± 11 (n and x = 5)	1.4 ± 0.4 (n and x = 5)	n = 14, x = 10
Anaphase bipole ablation	2.7 ± 0.3	18 ± 3	75 ± 10	3.0 ± 0.3	n = 10, x = 6
Anaphase bipole control	0.8 ± 0.2	n/a[b]	n/a[b]	n/a[b]	n = 10, x = 6
Monopole ablation	3.7 ± 0.3	8 ± 2	48 ± 7	2.2 ± 0.2	n = 37, x = 19
Monopole control	1.5 ± 0.2	66 ± 17[a]	53 ± 10	1.1 ± 0.2	n = 7, x = 6
Non-k-fiber microtubule bundles in monopoles	13 ± 1	3 ± 1	ND[c]	ND[c]	n = 12, x = 5
Recruited GFP-Arp1A in bipoles	2.6 ± 0.4	14 ± 3	32 ± 3	1.4 ± 0.2	n = 8, x = 6
Recruited GFP-NuMA in bipoles	1.9 ± 0.1	8 ± 1	71 ± 6	2.0 ± 0.1	n = 43, x = 14
Recruited GFP-NuMA in monopoles	2.9 ± 0.3	32 ± 2	37 ± 5	1.6 ± 0.2	n = 23, x = 7
DsRed-p150[217-548] overexpression	n/a[d]	122 ± 24 (post-ablation time without response)	n/a[d]	n/a[d]	n = 31, x = 11

Data are presented as mean ± SEM. See also Figs. 1–3 and 5. n/a, not applicable.
[a]Control delay time is the interval between the end of ablation and the first subsequent poleward motion of control unmanipulated chromosomes neighboring the ablation site.
[b]Because anaphase movement is dominantly poleward, these control measurements are not applicable.
[c]We did not measure duration and magnitude of the movement for non–k-fiber bundles since we were able to only briefly track the minus end after ablation.
[d]Because we did not see any consistent poleward response in cells inhibited with the p150 fragment, these measurements are not applicable.

were pulled toward spindle poles (Fig. 1 C and Video 2). In fact, chromatids with severed k-fibers moved poleward significantly faster than those with uncut k-fibers (Fig. 2 B), suggesting that a different mechanism powered their segregation. In addition, transport speeds were very similar from trace to trace (Fig. 2 B), consistent with a single mechanism powering the poleward transport response. Finally, transport speeds were faster at anaphase than at metaphase (2.7 ± 0.3 μm/min; Table 1), indicating that opposing force from a sister k-fiber can slow the poleward transport response during metaphase.

To test whether other interactions with the sister half-spindle can meaningfully oppose the poleward transport force, we generated monopolar spindles (where such interactions are eliminated) by inhibiting Eg5 with 5 μM S-trityl-L-cysteine (STLC). After ablation, severed k-fibers and associated chromosomes were abruptly pulled poleward (Fig. 1 D). As in metaphase and anaphase bipoles, chromosomes in monopolar spindles ultimately resumed normal movements (Fig. 2 C). However, poleward transport speeds after ablation (3.7 ± 0.3 μm/min) were significantly higher than in metaphase or anaphase bipoles (Fig. 1 D, Fig. 2 C, Table 1, and Video 3). In an anaphase bipolar spindle, therefore, the sister half-spindle still contributes resistance to poleward transport. In established bipolar spindles treated with STLC, the poleward transport force pulled chromosomes at 2.7 ± 0.3 μm/min (15 ablations in six cells): this is faster than in untreated bipolar spindles (Table 1), indicating that cross-linking by Eg5 may oppose transport in bipolar spindles, but is significantly slower than in monopolar spindles (Table 1), indicating that a monopolar architecture lacking sister half-spindle forces permits faster poleward transport independent of Eg5 activity. Moreover, the response in monopolar spindles, without sister half-spindle forces, confirms that the response force pulls, rather than pushes, on chromosomes.

We next investigated the strength of the poleward transport force relative to forces exerted directly on chromosomes as they move through the spindle. We eliminated the latter by ablating bundles of nonkinetochore microtubules in monopolar spindles, where these bundles were easiest to target. After severance, non–k-fiber microtubule bundles were pulled poleward with their minus ends leading, just as ablated k-fiber stubs were (Fig. 1 E and Video 4). Therefore, the poleward transport response does not require molecular loading at the kinetochore or k-fiber–specific proteins (Royle et al., 2005; Bird and Hyman, 2008; Meunier and Vernos, 2011; Sturgill and Ohi, 2013): it not only acts on all spindle architectures tested (Fig. 1, B–D), but also on all microtubule populations tested (Fig. 1, B and E). Non–k-fiber bundles moved poleward more than threefold faster than k-fiber stubs (13 ± 1 μm/min; Table 1), suggesting that forces exerted directly on chromosomes (e.g., from drag or chromokinesins) significantly oppose poleward transport. Thus, the poleward transport force is similar in magnitude to opposing forces on chromosomes, but can overpower them to dictate transport direction and preserve the mechanical connection between chromosome and pole.

Dynein powers the poleward transport response

Collectively, the characteristics of the poleward transport response suggest it is powered by a minus end–directed microtubule motor: after a delay, force generation begins abruptly and is active, fast, and processive. We suspected that dynein, which can slide microtubules to poles, powered the poleward transport response. Indeed, functional inhibition of dynein by overexpression of a dominant-negative p150 fragment (Quintyne and Schroer, 2002) resulted in absent or long-delayed incorporation of k-fiber stubs after ablation (Fig. 3 and Video 5). Free minus ends were tracked for an average of 122 ± 24 s after ablation
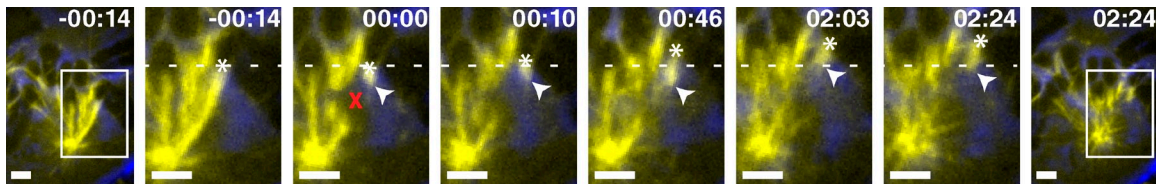
Figure 3. Dynein function is required for the poleward transport response. Time-lapse live images of a metaphase GFP–α-tubulin PtK2 spindle (phase contrast, blue; GFP–α-tubulin, yellow) response to k-fiber laser ablation when dynein cargo binding is inhibited by transfection of a dominant-negative p150 fragment. After laser ablation (X), the targeted k-fiber rotates (00:00–00:10) and splays (e.g., 02:03). No significant poleward movement of the newly generated k-fiber minus ends (arrowhead) and attached chromosome (kinetochore marked by asterisk) is observed. Minus ends are not reincorporated into the spindle by 02:24 (compare with delays in Fig. S1 B) despite nearby microtubule populations (e.g., 00:46). The spindle is fragmented and multipolar, as described after transfection with this p150 fragment (Quintyne and Schroer, 2002). Dotted line indicates the position of the kinetochore end of the ablated k-fiber immediately before ablation. Time is in min:s, with frame captured immediately after ablation set to 00:00. Bars, 2 µm. See also Video 5.

without displaying poleward movement or minus end reincorporation (Table 1). Both direct dynein inhibition and perturbed spindle microtubule architecture (e.g., a perturbed microtubule network for dynein to walk along) may contribute to the loss of poleward transport. Thus, dynein powers the poleward transport response.

Poleward force is exerted specifically on microtubule minus ends

To investigate the physical mechanism of dynein-powered poleward transport, we probed whether and how the response (displacement, timescale, and speed) varied spatially with the location of new minus ends. We focused on monopolar spindles because they displayed the most marked response to ablation and are in an experimentally tractable steady state. The response to new minus ends was robust: we observed fast poleward transport of 37 out of 40 ablated k-fibers in 19 cells. The magnitude of poleward movement correlated with the distance of the cut site from the pole (Table 2 and Fig. S1 A), suggesting that the poleward transport force pulls k-fiber stubs to the spindle pole.

Consistent with the idea that polar microtubule tracks guide post-ablation transport, the initiation of poleward movement sometimes coincided with visible contact between a k-fiber stub and neighboring microtubules (Fig. S2 and Video 2). In addition, very short stubs (<1 µm) displayed a longer delay between ablation and poleward transport initiation (Table 2 and Fig. S1 B). Because they sterically sample smaller volumes, short k-fiber stubs may have a lower probability of contacting microtubule tracks for dynein to walk along. For longer stubs, this correlation was absent, but the existence of an average 8-s delay (Table 1) suggested that the poleward force was not present on the k-fiber before ablation; if that were the case, movement would have begun immediately.

The delay is consistent with ablation-triggered recruitment of force-generating machinery to new, ablation-created structures

such as the new minus ends. This suggestion that motor machinery is targeted to specific microtubule structures raised the question of where on transported microtubules force is exerted. A model of microtubule sliding powered by dynein at points of lateral microtubule contact would predict force generation all along the microtubule (Merdes et al., 2000; Radulescu and Cleveland, 2010). In contrast, we found that the speed of the poleward transport response does not correlate with the length of the k-fiber stub (Table 2 and Fig. S1 C), suggesting that the force driving transport is not generated all along the stub. (Slower speeds of ablated k-fibers compared with non–k-fiber bundles suggest that dynein can move faster under a lighter load, so that an increase in number of motors and corresponding decrease in load per motor would be capable of increasing the transport speed.) Because speed does not increase with stub length, force may be generated at its minus end, a structure singular to each ablated microtubule bundle. Consistent with force at minus ends dominating mechanical interactions along the k-fiber, the severed stub rapidly pivoted 180° during rare (<5% of cases) observations of post-ablation movement toward the opposite pole (similar to observations by Dick and Gerlich [2013]), likely along an atypically polarized microtubule track (Fig. S3 and Video 6). Given these observations, we hypothesized that the dynein-powered poleward transport force is in fact a minus end poleward transport force, which identifies and pulls free minus ends as cargo.
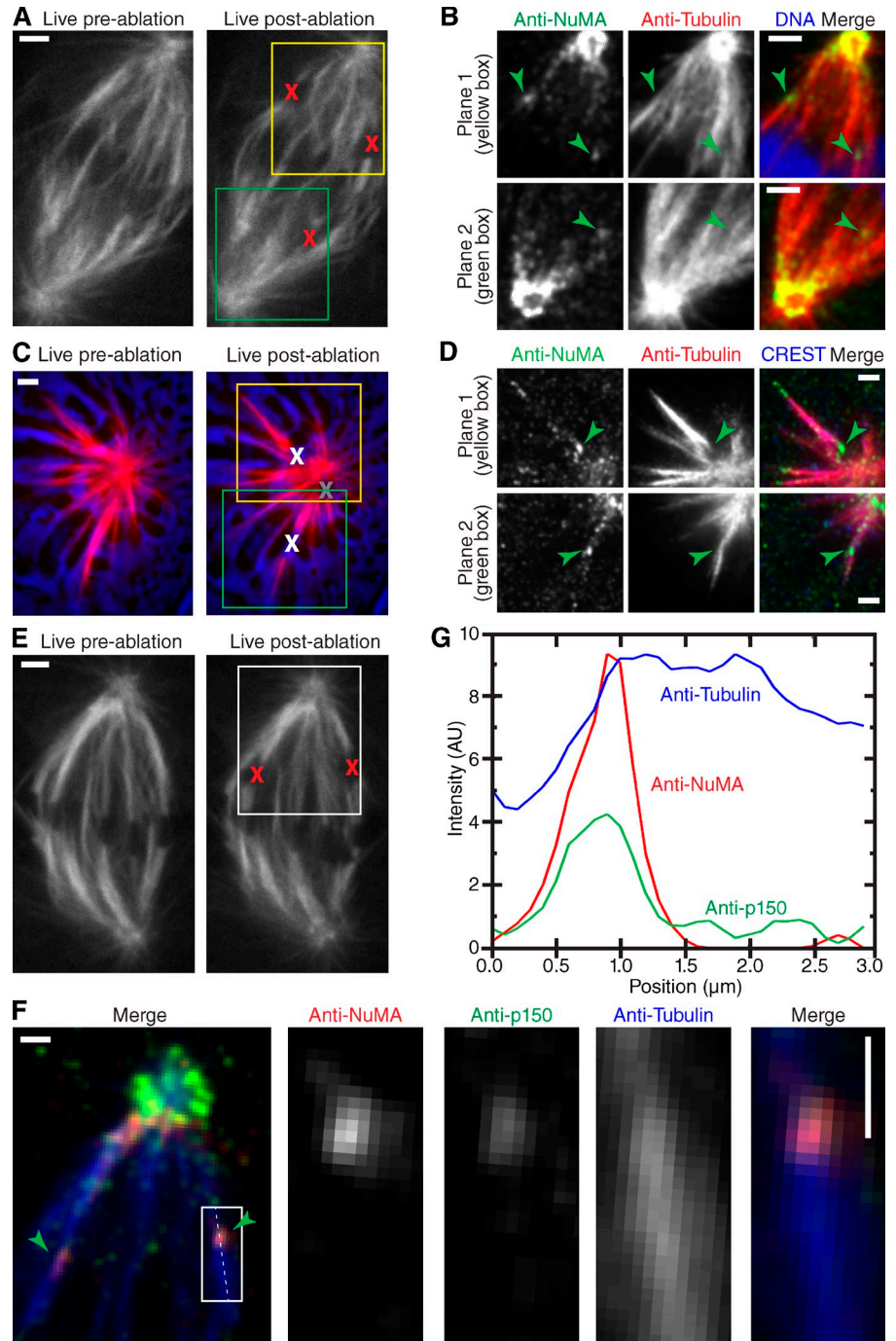
To test whether force generation at minus ends is necessary for k-fiber stub poleward transport, we performed a second ablation to destroy the stub minus end, after poleward transport began but before the minus end was indistinguishable from surrounding microtubules. Ablation of the stub minus end abolished movement toward the pole, both in bipolar and monopolar spindles; movement began again after a delay (Figs. 1 F and 2 E and Video 7). Although current data cannot resolve whether few or most minus ends within a k-fiber productively engage

Table 2. Probing correlations between ablation location and the k-fiber poleward transport response

First parameter	Second parameter	Correlation coefficient	P-value
Magnitude of poleward movement	Distance of cut site from pole	0.42	0.01[a]
Delay before poleward movement	Length of k-fiber stub	−0.46	0.0039[a]
Speed of poleward movement	Length of k-fiber stub	0.0092	0.96

All data collected in monopolar spindles. See also Fig. S1.
[a]P-values that are significant (≤0.01).

Figure 4. NuMA and dynactin are recruited specifically to newly generated minus ends. (A) Live images of a GFP–α-tubulin PtK2 spindle immediately before and after k-fiber ablation at targeted sites (X). (B) Representative immunofluorescence image of NuMA, α-tubulin, and DNA (Hoescht) in cell from A, fixed after ablation. NuMA (arrowheads) localizes to new minus ends. (C) Live images of a GFP–α-tubulin PtK2 monopolar spindle (phase contrast [blue] to identify chromosome locations; α-tubulin, red) immediately before (left) and after (right) ablation of non–k-fiber bundles (each ablation site marked by white X). One k-fiber is also ablated (gray X). (D) Representative immunofluorescence image of NuMA, α-tubulin, and kinetochores (CREST) in two planes of same cell from C, fixed after ablation. NuMA (arrowheads) localizes to new minus ends. In Plane 1, new minus ends are not yet reincorporated into the spindle; in Plane 2, the new minus ends appear to have moved poleward along another microtubule bundle (note contact between the microtubule bundles at the new NuMA-marked minus ends). (E) Live images of a GFP–α-tubulin PtK2 spindle immediately before and after k-fiber ablation at targeted sites (X). (F) Representative immunofluorescence images of NuMA, dynactin subunit p150, and α-tubulin in cell from E, fixed after ablation. Arrowheads mark NuMA and p150 recruited to new minus ends. The ablated k-fiber on the left has associated with other microtubules before fixation, whereas the minus ends of the ablated k-fiber on the right remain unattached. (G) Line scan analysis of NuMA, dynactin subunit p150, and α-tubulin intensity along dashed line in F. NuMA and p150 co-localize at new microtubule minus ends, and loss of tubulin intensity confirms ablation. Representative example of five ablations in four cells. Bars: (A–E) 2 µm; (F) 1 µm.

A Live pre-ablation | Live post-ablation
B Anti-NuMA | Anti-Tubulin | DNA Merge
Plane 1 (yellow box) | Plane 2 (green box)
C Live pre-ablation | Live post-ablation
D Anti-NuMA | Anti-Tubulin | CREST Merge
Plane 1 (yellow box) | Plane 2 (green box)
E Live pre-ablation | Live post-ablation
G Anti-Tubulin | Anti-NuMA | Anti-p150
F Merge | Anti-NuMA | Anti-p150 | Anti-Tubulin | Merge

during poleward force generation, the loss of force generation after minus end ablation suggests that mechanical engagement at the k-fiber minus end is essential for the poleward transport response. Thus, although forces may also be generated all along the k-fiber (Nicklas et al., 1982; Maiato et al., 2004; Vladimirou et al., 2013), they were not sufficient to power the rapid stub and chromosome transport we observed.

Dynactin and NuMA identify new minus end structures as cargo within seconds and processively escort them to poles

If dynein and its binding partners identify and pull free microtubule minus ends, rather than nonpreferentially exerting sliding forces all along microtubule lengths, we would expect them to specifically localize to new minus ends. To test for such localization, we fixed metaphase bipolar cells immediately after ablation and performed immunofluorescence staining. We first stained for NuMA (Fig. 4, A and B), which showed striking localization at new minus ends as early as 15 s after ablation, the fastest we were able to fix after ablation. When we ablated non–k-fiber bundles, we found that NuMA also localized specifically to these newly created minus ends (Fig. 4, C and D). Thus, the free minus ends of both k-fiber and non–k-fiber microtubule bundles recruit NuMA.

To investigate whether dynein accompanied NuMA and was selectively enriched at new minus ends, we stained after ablation for p150 (also called p150[Glued]), a component of the dynein

adapter complex dynactin (Gill et al., 1991), which is required for NuMA to associate with dynein (Merdes et al., 2000). Indeed, p150 colocalized with NuMA selectively at minus ends of severed fibers (Fig. 4, E–G). The fact that NuMA and dynactin specifically localize to minus end structures is consistent with data suggesting that dynein generates force at the minus end itself, as opposed to all along the microtubule (Tables 1 and 2; Figs. 1 F, 2 E, S1 C, and S3; and Videos 6 and 7).

After immunofluorescence indicated that NuMA and dynactin specifically mark new minus ends as motor cargo, we wondered how quickly they identified minus ends and if and where they subsequently moved. We turned to live imaging to understand the timescale of dynein/dynactin and NuMA recruitment and their dynamics and processivity relative to the minus end poleward transport response. Another component of the dynactin complex, Arp1A (Lees-Miller et al., 1992), was quickly recruited to sites of ablation in metaphase bipoles, within an average of 14 ± 3 s (Fig. 5, A and B; Table 1; and Video 8). GFP-Arp1A puncta moved at speeds (2.6 ± 0.4 µm/min; Table 1) similar to the metaphase k-fiber poleward transport response, and they continued processively until they became indistinguishable from the pole. To determine if Arp1A puncta colocalized with minus ends throughout their trajectories, we ablated k-fibers in cells expressing mCherry-tubulin and GFP-Arp1A. Arp1A puncta appeared at new minus ends and moved together with them toward poles (Fig. 5, C and D; and Video 9).

GFP-NuMA was visible at ablation sites an average of 8 ± 1 s after ablation (Table 1; Fig. 5, E and F; and Video 10) in metaphase bipoles, more quickly than GFP-Arp1A recruitment was detectable. This difference may reflect temporal recruitment order or may result from higher contrast GFP-NuMA signal. The recruitment of GFP-NuMA occurred before the initiation of poleward movement of severed k-fibers in metaphase bipoles (15 ± 4 s; Table 1). In some cases, GFP-NuMA was detectable at the ablation site for up to 40 s before it moved poleward (Fig. 5 G and Fig. S4). Like GFP-Arp1A, recruited GFP-NuMA moved poleward at speeds in keeping with the minus end transport response until it merged with NuMA structures at the pole (1.9 ± 0.1 µm/min; Table 1 and Fig. 5, E and F). The speed of movement decreased as the recruited NuMA neared the spindle pole (Fig. 5, F and G). Notably, the speed of microtubules in *Xenopus laevis* extract spindles decreases near poles in a dynein-dependent manner (Burbank et al., 2007; Yang et al., 2008). Consistent with our characterization of k-fiber movement during minus end poleward transport, the poleward movement of GFP-NuMA in monopolar spindles was significantly faster (2.9 ± 0.3 µm/min; Table 1) than in bipolar spindles. Lastly, in cells expressing mCherry-NuMA and GFP-Arp1A, NuMA and Arp1A puncta colocalized and moved together to poles (Fig. S5).

In sum, the data indicate that throughout mitosis, dynein/dynactin and NuMA rapidly and specifically identify free microtubule minus ends and pull them as cargo to the spindle pole, generating enough force to maintain k-fiber anchorage and move chromosomes.

Discussion

The maintenance of focused poles is central to spindle architecture and function. Here, we sever spindle microtubules using laser ablation to create detached k-fiber and non–k-fiber microtubules. We find that dynein/dynactin and NuMA rapidly, efficiently, and specifically identify the free minus ends of these detached microtubules and processively pull minus ends as cargo to poles. Although this force acts at minus ends, it can overpower opposing pulls all along microtubules and on chromosomes and power spindle self-repair, prioritizing the structural reintegration of minus ends. We demonstrate not only that a force exerted on microtubule minus ends can move and segregate chromosomes but also that this poleward minus end force overpowers canonical forces on chromosomes exerted at plus ends. Minus end reintegration maintains spindle architecture on a faster timescale (seconds) than chromosome movement (minutes), ensuring that chromosomes remain bioriented and are transported to poles at anaphase.

Free microtubule minus ends are specific cargoes for dynein force generation

The data herein suggest a model for spindle architecture maintenance by efficient cellular identification and poleward transport of free microtubule minus ends (Fig. 6 A). Within seconds of their creation, new minus ends recruit NuMA and dynein/dynactin. Minus ends remain detached from the spindle until they come into contact with a neighboring spindle microtubule track seconds later. Upon contact, dynein walks processively poleward along this track, pulling its microtubule minus end cargo (Fig. 6 B). Together, complexes of NuMA, dynactin, and dynein may act as a physical tether between a microtubule track (bound to dynein) and microtubule cargo (bound to NuMA) and power the poleward transport of spindle microtubule minus ends. Estimation of the frictional force experienced by a microtubule bundle moving at the speeds we observe suggests that multiple dynein motors are likely responsible for this poleward force on minus ends (Nicklas, 1988; Shubeita et al., 2008; Shimamoto et al., 2011). Targeting dynein molecules specifically to minus ends, rather than all along the microtubule, provides a simple and intuitive mechanism for clustering minus ends into poles (Burbank et al., 2007).

Newly created microtubule minus ends are biochemically marked within seconds

NuMA and dynein are thought to incorporate kinetochore-nucleated k-fibers during spindle formation (Merdes et al., 2000; Khodjakov et al., 2003). Yet when NuMA is inhibited, two focused spindle poles still form; only later do poles defocus (Silk et al., 2009). The present study helps reconcile these findings. Based on the observation that NuMA rapidly and robustly localizes to new minus ends, we hypothesize that spindle maintenance involves not only NuMA's canonical role as a tethering "glue" at poles (Merdes et al., 1996; Silk et al., 2009) but also NuMA-mediated capture and poleward transport of spindle microtubule minus ends (Khodjakov et al., 2003) that are created or lost from poles. NuMA may act as a tether in two places: between a
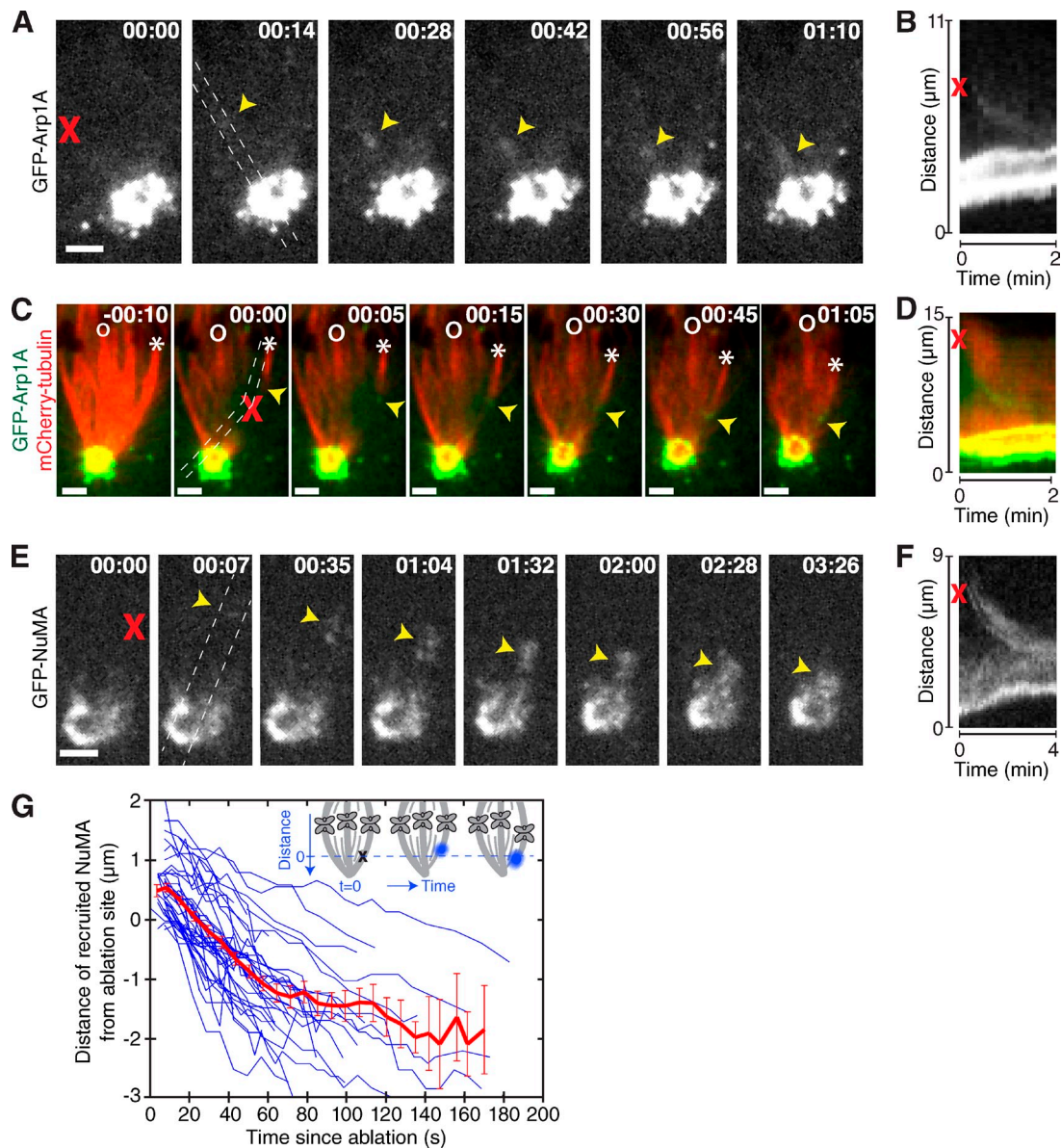
Figure 5. **Dynactin and NuMA identify new minus ends within seconds and escort them to spindle poles.** (A and E) Representative time-lapse live images of PtK2 cells expressing GFP-Arp1A (A) or GFP-NuMA (E). Arp1A and NuMA (arrowheads) are recruited to the sites of ablation (X) within seconds and move rapidly and processively poleward. GFP-Arp1A and GFP-NuMA puncta move poleward until they are indistinguishable from poles. Time is in min:s, with frame captured immediately after ablation set to 00:00. See also Videos 8 and 10. (B and F) Kymographs along poleward path of GFP-Arp1A (B) or GFP-NuMA (F) puncta, between dashed lines in A and E. Note that the spindle pole itself (bright signal along bottom of kymograph) moves upward during minus end poleward transport, consistent with a reactive force on the spindle pole as the ablated k-fiber is pulled downward via a pole-connected track. (C) Representative time-lapse live images of cells expressing mCherry-tubulin and GFP-Arp1A reveal that recruited Arp1A (arrowheads) localizes at and moves with new microtubule minus ends after ablation (at X). The kinetochore of the ablated k-fiber is marked by an asterisk and a neighboring non-ablated kinetochore is marked by o. See also Video 9. (D) Kymograph along poleward path between dashed lines in C of ablated mCherry-tubulin k-fiber and GFP-Arp1A puncta. (G) Distance of GFP-NuMA puncta from ablation site as puncta move processively poleward after ablation. In some cases, stationary GFP-NuMA is detectable at the ablation site for up to 40 s before it moves poleward (see also Fig. S4). Red trace indicates the mean (error bars represent SEM) of 43 individual responses (blue traces). On average, the recruited GFP-NuMA first appears ~0.5 µm farther away from the pole than the site of ablation, which is expected given an ablation area of ~1 µm (see Materials and methods).

minus end and its microtubule track, and between that track and the pole. In retrospect, earlier visualization of NuMA along the length of kinetochore-nucleated k-fibers, not only at their tips (Khodjakov et al., 2003), may reflect the tapered nature of these fibers. By creating synchronized minus ends, the targeted ablation approach used here allows us to dissect the location of dynein force generation and reveals specific recruitment and activity of dynein/dynactin and NuMA at microtubule minus ends

(Fig. 6 B). Together, the creation of synchronized minus ends by ablation and their subsequent molecular marking by the cell offer a way to image spindle microtubule minus ends—a long-standing challenge.

This study places an upper bound of 8 s on the time required to establish distinct biochemistry at free minus ends and it raises the question of how microtubule minus ends are specifically identified within the spindle body. We consider two models and
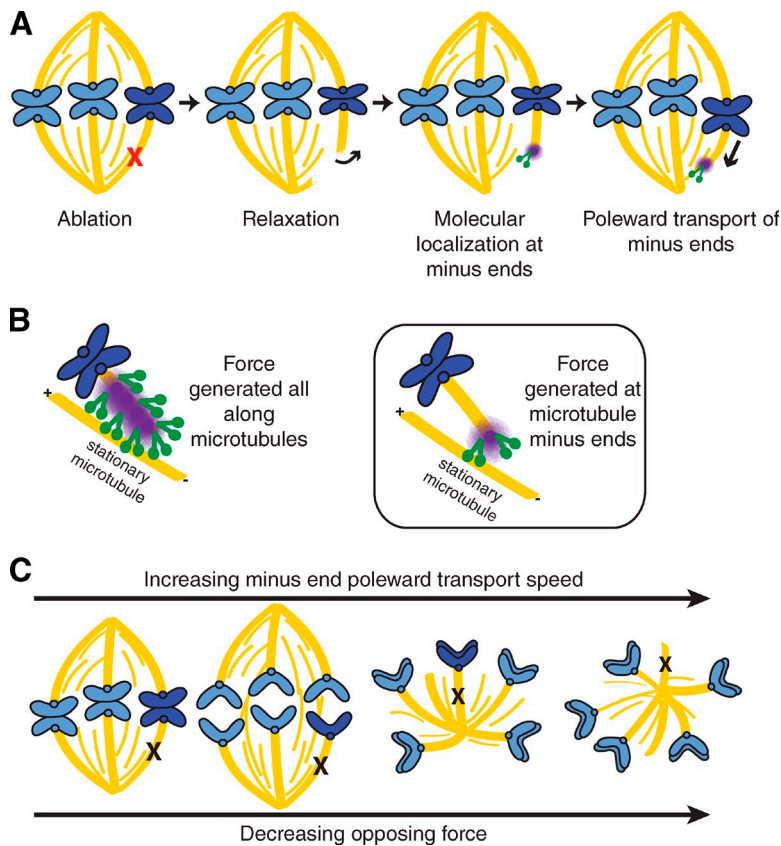
Figure 6. **Forces on new microtubule minus ends move chromosomes and maintain spindle organization.** (A) Model for rapid identification and organization of new spindle microtubule minus ends. NuMA (purple) and dynein/dynactin (green) rapidly localize to new microtubule minus ends after ablation (red X). Once dynein comes into contact with neighboring microtubules, it walks processively poleward along them, pulling the new minus ends as cargo and moving the attached chromosome (dark blue chromosome). (B) Imaging and biophysical analysis suggest that poleward transport is powered by force generation at minus ends of cargo microtubules. (C) Comparing the magnitudes of spindle forces. In all spindle structures studied, the poleward transport force overpowers other forces on chromosomes and/or microtubule bundles to move them toward poles. However, the speed of poleward movement increases as opposing forces decrease. Thus, the poleward transport force dominates but is tuned to other spindle forces, allowing it to maintain pole architecture without disrupting spindle integrity.

cannot currently distinguish between them. First, dynein could walk along microtubules until it runs out of track, delivering dynactin and NuMA to minus ends. In this scenario, dynein molecules first use the k-fiber as a track, pile up at the minus end without falling off—the basis for minus end selective identification—and later hold on to the minus end as cargo. Alternatively, soluble NuMA and dynein/dynactin may be recruited selectively to minus ends from the cytoplasm, binding either directly or indirectly to minus ends. NuMA binds microtubules directly (Du et al., 2002; Haren and Merdes, 2002), and previous work has suggested that NuMA can localize to minus ends independently of dynein (Heald et al., 1997). After ablation, then, NuMA may recruit dynactin and dynein specifically to minus ends, consistent with the faster recruitment we observe for NuMA than dynactin (Table 1). If indirect, binding may occur through one of the two known direct minus end–interacting partners, the γ-tubulin ring complex (Zheng et al., 1995) or the recently characterized CAMSAP family (Meng et al., 2008), which localizes to interphase microtubule minus ends created by ablation (Jiang et al., 2014).

Self-repair is tuned to competing forces and dynamically maintains spindle mechanical integrity

This work identifies an unexpected mechanism of chromosome translocation mediated by a poleward force on k-fiber minus ends. The minus end poleward force is similar in magnitude to other forces on chromosomes but capable of directionally dominant transport (Fig. 6 C), allowing it to (a) work in tandem with

other forces without being so strong as to disrupt spindle architecture but (b) prioritize correct integration of free minus ends. Minus ends are relatively stable and thus preserve structural memory, and a uniquely fast cellular response to free minus ends may preserve bipolar structure and chromosome biorientation. As such, minus end transport forces may be tuned to competing spindle forces—strong and fast enough to ensure the accurate integration of k-fiber minus ends into poles given the strength and dynamics of opposing forces on chromosomes.

Spindle microtubules need to be continuously organized as minus ends are created or exposed by microtubule nucleation, microtubule-severing enzymes, augmin-mediated branching events (Goshima et al., 2008), or detachment from previous structures (Lancaster et al., 2013; Petry et al., 2013). The findings herein open new questions: whether NuMA and dynein localize to the minus ends of all spindle microtubules and whether all populations of spindle minus ends are rapidly transported by this poleward force. If the poleward transport machinery recognizes only a subset of minus ends, it could discriminate on the basis of structure (e.g., minus ends of bundled microtubules) or biochemistry (e.g., "naive" ablation-created minus ends with exposed interfaces not yet masked by minus end binding proteins).

Paradoxically, the mitotic spindle is a highly dynamic and yet mechanically robust macromolecular machine. Spindle poles, for example, persist for lifetimes longer than their components and are both flexible and mechanically strong, as illustrated by manipulation experiments (Nicklas and Staehly, 1967; Begg and Ellis, 1979; Charlebois et al., 2011). Rapid-acting, strong forces that continuously maintain spindle integrity could

resolve this paradox. The robust minus end transport response we observe represents one such mechanism for maintaining chromosome anchorage and spindle architecture by dynamic self-repair: rapid error detection (of free minus ends) and resolution (via dominant poleward transport).

Materials and methods

Cell culture and transfection

PtK2 GFP–α-tubulin cells (stable line expressing human α-tubulin in pEGFP-C1; Takara Bio Inc.; a gift from A. Khodjakov, Wadsworth Center, Albany, NY; Khodjakov et al., 2003) and PtK2 cells were cultured in MEM (Invitrogen) supplemented with sodium pyruvate (Invitrogen), nonessential amino acids (Invitrogen), penicillin/streptomycin, and 10% qualified and heat-inactivated fetal bovine serum (Invitrogen). Cells were plated on #1.5 25-mm coverslips (HCl-cleaned and poly-L-lysine coated) and imaged in Leibovitz's L-15 medium with L-glutamine without phenol red (Invitrogen) with antibiotics and serum as for cell culture. PtK2 cells were transfected with mCherry-tubulin (human α-tubulin in pmCherry-C1; Takara Bio Inc.; a gift from M. Davidson, Florida State University, Tallahassee, FL), GFP-NuMA(N1) (human NuMA in pEGFP-N1; Takara Bio Inc.; a gift from D. Compton, Dartmouth Medical School, Hanover, NH; Kisurina-Evgenieva et al., 2004), mCherry-NuMA (from GFP-NuMA(N1); we replaced GFP with mCherry between AgeI and NotI sites), or GFP-Arp1A (human Arp1A in a pBABE variant; Addgene; a gift from I. Cheeseman, Whitehead Institute, Cambridge, MA; Kiyomitsu and Cheeseman, 2012) using Fugene6 (Promega) and imaged 36–48 h after transfection.

Drug treatment

To make monopolar spindles, STLC (Sigma-Aldrich) was added to cells in MEM (see previous paragraph) 20 min before imaging at 5 µM (10 mM DMSO stock). Cells were imaged in L-15 (see previous paragraph) containing 5 µM STLC. To probe bipolar spindles with inhibited Eg5, we added 5 µM STLC after spindle formation, which preserves bipolarity (Cameron et al., 2006).

Dynein perturbation

To perturb dynein via dominant-negative overexpression, DsRed-p150[217–548] (amino acids 217–548 of chicken p150 in pDsRed-N1; Takara Bio Inc.; a gift from T. Schroer, Johns Hopkins University; Baltimore, MD; Quintyne and Schroer, 2002) was transfected with Fugene6 72–96 h before imaging. Dynein-inhibited cells were identified via DsRed fluorescence and spindle morphology: cells with fragmented, multipolar spindles (Quintyne and Schroer, 2002) indicative of dynein loss of function were specifically selected. We mildly compressed (Dumont and Mitchison, 2009) some of the dynein-inhibited spindles imaged (including the one in Fig. 3 and Video 5) to keep them in focus and to increase contact probabilities between new minus ends and neighboring microtubules. Both k-fiber and non–k-fiber bundles were laser ablated.

Immunofluorescence

For immunofluorescence of individual cells after ablation, cells were live imaged on coverslips photoetched with a labeled grid (Thermo Fisher Scientific). After ablation, cells were fixed in 95% methanol with 5 mM EGTA for 3 min. The time between laser ablation and fixation was usually ∼30 s, but could be as fast as 15 s. The following antibodies and dyes were used: mouse anti–α-tubulin DM1α (1:1,000; Sigma-Aldrich), rabbit anti-NuMA (1:300; Novus Biologicals), mouse anti–p150-Glued (1:500; BD), human anti-centromere protein (CREST; 1:25; Antibodies, Inc.), mouse anti–α-tubulin DM1α conjugated to Alexa 488 (1:50; Cell Signaling Technology), fluorescent secondary antibodies (1:500; Invitrogen), and Hoescht 33342 (Sigma-Aldrich). After staining, we identified the ablated cell using the coverslip grid.

Imaging and laser ablation

Live imaging was performed on an inverted microscope (Eclipse Ti-E; Nikon) with a spinning disk confocal (CSU-X1; Yokogawa Electric Corporation), head dichroic Semrock Di01-T405/488/561GFP (except Di01-T488 for GFP-NuMA-only, GFP-Arp1A-only, Fig. 1 F, and Video 5), 488-nm (120 mW) and 561-nm (150 mW) diode lasers, emission filters ET525/36M (Chroma Technology Corp.) for GFP (except ET500LP for GFP-NuMA-only, GFP-Arp1A-only, Fig. 1 F, and Video 5) or ET630/75M for mCherry, and an iXon3 camera (Andor Technology). Cells were imaged by phase

contrast (400–500-ms exposures) and fluorescence (75–500-ms exposures) every 3.5–14 s with a 100× 1.45 Ph3 oil objective through a 1.5× lens yielding 105 nm/pixel at bin = 1 (Metamorph 7.7.8.0; Molecular Devices). Figs. 5 C and S5 and Video 9 were collected at bin = 2. Cells were imaged at 29–31°C in a homemade heated aluminum coverslip holder, using the Perfect Focus System (Nikon). Targeted laser ablation (several 3-ns pulses at 20 Hz) using 551- (if only GFP imaged) or 514-nm (if GFP and mCherry imaged) light was performed using a galvo-controlled MicroPoint Laser System (Photonic Instruments) operated through Metamorph. Based on fluorescence imaging, we estimate the diameter of the ablation site at ∼1 µm. K-fiber ablation was verified by observed loss of mechanical tension across the centromere, depolymerization of the uncapped microtubule plus end, and free reorientation of the severed k-fiber stub after ablation (Fig. 1 B). For cells fixed after ablation, loss of tubulin staining at the ablation site confirmed k-fiber and non–k-fiber severance (Fig. 4).

Data analysis

Chromosome position data were generated by manual tracking of k-fiber plus ends, ablation sites, and spindle poles in live-imaged GFP–α-tubulin PtK2 cells, using overlaid GFP–α-tubulin and phase-contrast time-lapse videos in a home-written MatLab (R2012a Version 7.4) program. As controls, we also tracked neighboring k-fiber plus ends (of unmanipulated chromosomes in metaphase and monopolar spindles, and of the paired sister chromatids in anaphase spindles). We manually selected the start and end times of the poleward transport response (for ablated k-fibers) or the first poleward movement after ablation (for control chromosomes) by examining plots of k-fiber plus end position over time and choosing the segment over which poleward motion was processive, and we used these times and positions to calculate mean speeds. We calculated the delay times as the difference between the first frame after ablation and the first frame of this sustained poleward response. For non–k-fibers, we manually tracked the position of their new minus ends as long as possible.

Line scan analysis of immunofluorescence colocalization was performed using the plot profile function of ImageJ with a line width of 1 pixel.

Kymographs of GFP-Arp1A and GFP-NuMA puncta and pole position over time were generated in ImageJ. A second home-written MatLab program generated fluorescence intensity line scans for each frame from the kymograph. Using each sequence of line scans, the peaks indicating the positions of GFP-Arp1A/GFP-NuMA puncta and the spindle pole were manually selected, with the intensity maxima of these peaks used to indicate puncta positions. We defined the initial recruitment time of GFP-Arp1A/GFP-NuMA puncta as the first frame in which a clear peak was visible in the line scan. We continued to track puncta until their intensity peaks could not be clearly separated from those of the spindle poles. To calculate the distance of these peak positions from the ablation sites, we used the ablation targeting coordinates from Metamorph. For comparing the intensity of GFP-NuMA puncta recruited to sites of ablation to other puncta, we calculated the fold difference in the mean integrated intensity of at least four puncta in each cell at sites/times without ablation and the integrated intensity of puncta recruited after ablation.

Data are expressed as mean ± SEM. Calculations of correlation coefficients (Pearson's r) and p-values were performed in MatLab. For calculating mean traces in Fig. 5 G, data from all traces were collected into 10-s-wide bins in time and the mean position within this bin was calculated.

Video preparation

To detect the details of the cellular response to ablation while minimizing photodamage from frequent imaging, cells were imaged less frequently before ablation and more frequently immediately after ablation. For the videos to play back at a constant 30× speed relative to real time, frames are shown in the videos for a time inversely proportional to the rate at which they were collected.

Online supplemental material

Fig. S1 shows that ablation position affects the magnitude of movement and the delay before poleward transport, but not the transport speed. Fig. S2 uses an example to illustrate that the initiation of poleward transport immediately follows contact with neighboring microtubules. Fig. S3 shows the rare observation of a 180° pivot of the k-fiber stub and poleward transport to the opposite pole, suggesting that poleward force is not exerted all along the k-fiber. Fig. S4 shows that the recruitment of NuMA sometimes precedes its poleward movement. Fig. S5 shows that GFP-Arp1A and mCherry-NuMA colocalize at sites of ablation and move together to poles. Video 1 shows that laser ablation of a k-fiber triggers poleward chromosome movement in a metaphase bipolar spindle. Video 2

demonstrates that the poleward transport response persists into anaphase to segregate chromosomes. Video 3 shows that the poleward transport response is faster in monopolar spindles than in metaphase or anaphase. Video 4 illustrates that the poleward transport response occurs and is fastest for non–k-fiber microtubule bundles. Video 5 demonstrates that dynein function is required for the poleward transport response. Video 6 shows the rare observation of a 180° pivot of the k-fiber stub and poleward transport to the opposite pole, suggesting that force is not exerted all along the k-fiber. Video 7 suggests that the poleward transport response requires force generation at minus ends because ablation of the minus ends stops the response. Video 8 shows that GFP-Arp1A is recruited to sites of ablation and moves all the way to poles. Video 9 shows that GFP-Arp1A localizes specifically to new minus ends and moves with them. Video 10 shows that GFP-NuMA is recruited to sites of ablation and moves all the way to poles. Online supplemental material is available at http://www.jcb.org/cgi/content/full/jcb.201401091/DC1.

References

Begg, D.A., and G.W. Ellis. 1979. Micromanipulation studies of chromosome movement. I. Chromosome-spindle attachment and the mechanical properties of chromosomal spindle fibers. *J. Cell Biol.* 82:528–541. http://dx.doi.org/10.1083/jcb.82.2.528

Bird, A.W., and A.A. Hyman. 2008. Building a spindle of the correct length in human cells requires the interaction between TPX2 and Aurora A. *J. Cell Biol.* 182:289–300. http://dx.doi.org/10.1083/jcb.200802005

Brugués, J., V. Nuzzo, E. Mazur, and D.J. Needleman. 2012. Nucleation and transport organize microtubules in metaphase spindles. *Cell.* 149:554–564. http://dx.doi.org/10.1016/j.cell.2012.03.027

Burbank, K.S., T.J. Mitchison, and D.S. Fisher. 2007. Slide-and-cluster models for spindle assembly. *Curr. Biol.* 17:1373–1383. http://dx.doi.org/10.1016/j.cub.2007.07.058

Cameron, L.A., G. Yang, D. Cimini, J.C. Canman, O. Kisurina-Evgenieva, A. Khodjakov, G. Danuser, and E.D. Salmon. 2006. Kinesin 5–independent poleward flux of kinetochore microtubules in PtK1 cells. *J. Cell Biol.* 173:173–179. http://dx.doi.org/10.1083/jcb.200601075

Charlebois, B.D., S. Kollu, H.T. Schek, D.A. Compton, and A.J. Hunt. 2011. Spindle pole mechanics studied in mitotic asters: dynamic distribution of spindle forces through compliant linkages. *Biophys. J.* 100:1756–1764. http://dx.doi.org/10.1016/j.bpj.2011.02.017

Chen, W., and D. Zhang. 2004. Kinetochore fibre dynamics outside the context of the spindle during anaphase. *Nat. Cell Biol.* 6:227–231. http://dx.doi.org/10.1038/ncb1104

Dick, A.E., and D.W. Gerlich. 2013. Kinetic framework of spindle assembly checkpoint signalling. *Nat. Cell Biol.* 15:1370–1377. http://dx.doi.org/10.1038/ncb2842

Dionne, M.A., L. Howard, and D.A. Compton. 1999. NuMA is a component of an insoluble matrix at mitotic spindle poles. *Cell Motil. Cytoskeleton.* 42:189–203. http://dx.doi.org/10.1002/(SICI)1097-0169(1999)

Du, Q., L. Taylor, D.A. Compton, and I.G. Macara. 2002. LGN blocks the ability of NuMA to bind and stabilize microtubules. A mechanism for mitotic spindle assembly regulation. *Curr. Biol.* 12:1928–1933. http://dx.doi.org/10.1016/S0960-9822(02)01298-8

Dumont, S., and T.J. Mitchison. 2009. Compression regulates mitotic spindle length by a mechanochemical switch at the poles. *Curr. Biol.* 19:1086–1095. http://dx.doi.org/10.1016/j.cub.2009.05.056

Gaglio, T., A. Saredi, and D.A. Compton. 1995. NuMA is required for the organization of microtubules into aster-like mitotic arrays. *J. Cell Biol.* 131:693–708. http://dx.doi.org/10.1083/jcb.131.3.693

Gaglio, T., M.A. Dionne, and D.A. Compton. 1997. Mitotic spindle poles are organized by structural and motor proteins in addition to centrosomes. *J. Cell Biol.* 138:1055–1066. http://dx.doi.org/10.1083/jcb.138.5.1055

Gatlin, J.C., A. Matov, A.C. Groen, D.J. Needleman, T.J. Maresca, G. Danuser, T.J. Mitchison, and E.D. Salmon. 2009. Spindle fusion requires dynein-mediated sliding of oppositely oriented microtubules. *Curr. Biol.* 19:287–296. http://dx.doi.org/10.1016/j.cub.2009.01.055

Gill, S.R., T.A. Schroer, I. Szilak, E.R. Steuer, M.P. Sheetz, and D.W. Cleveland. 1991. Dynactin, a conserved, ubiquitously expressed component of an activator of vesicle motility mediated by cytoplasmic dynein. *J. Cell Biol.* 115:1639–1650. http://dx.doi.org/10.1083/jcb.115.6.1639

Gordon, M.B., L. Howard, and D.A. Compton. 2001. Chromosome movement in mitosis requires microtubule anchorage at spindle poles. *J. Cell Biol.* 152:425–434. http://dx.doi.org/10.1083/jcb.152.3.425

Goshima, G., F. Nédélec, and R.D. Vale. 2005. Mechanisms for focusing mitotic spindle poles by minus end–directed motor proteins. *J. Cell Biol.* 171:229–240. http://dx.doi.org/10.1083/jcb.200505107

Goshima, G., M. Mayer, N. Zhang, N. Stuurman, and R.D. Vale. 2008. Augmin: a protein complex required for centrosome-independent microtubule generation within the spindle. *J. Cell Biol.* 181:421–429. http://dx.doi.org/10.1083/jcb.200711053

Haren, L., and A. Merdes. 2002. Direct binding of NuMA to tubulin is mediated by a novel sequence motif in the tail domain that bundles and stabilizes microtubules. *J. Cell Sci.* 115:1815–1824.

Heald, R., R. Tournebize, T. Blank, R. Sandaltzopoulos, P. Becker, A. Hyman, and E. Karsenti. 1996. Self-organization of microtubules into bipolar spindles around artificial chromosomes in *Xenopus* egg extracts. *Nature.* 382:420–425. http://dx.doi.org/10.1038/382420a0

Heald, R., R. Tournebize, A. Habermann, E. Karsenti, and A. Hyman. 1997. Spindle assembly in *Xenopus* egg extracts: respective roles of centrosomes and microtubule self-organization. *J. Cell Biol.* 138:615–628. http://dx.doi.org/10.1083/jcb.138.3.615

Jiang, K., S. Hua, R. Mohan, I. Grigoriev, K.W. Yau, Q. Liu, E.A. Katrukha, A.F. Altelaar, A.J. Heck, C.C. Hoogenraad, and A. Akhmanova. 2014. Microtubule minus-end stabilization by polymerization-driven CAMSAP deposition. *Dev. Cell.* 28:295–309. http://dx.doi.org/10.1016/j.devcel.2014.01.001

Khodjakov, A., L. Copenagle, M.B. Gordon, D.A. Compton, and T.M. Kapoor. 2003. Minus-end capture of preformed kinetochore fibers contributes to spindle morphogenesis. *J. Cell Biol.* 160:671–683. http://dx.doi.org/10.1083/jcb.200208143

Kisurina-Evgenieva, O., G. Mack, Q. Du, I. Macara, A. Khodjakov, and D.A. Compton. 2004. Multiple mechanisms regulate NuMA dynamics at spindle poles. *J. Cell Sci.* 117:6391–6400. http://dx.doi.org/10.1242/jcs.01568

Kiyomitsu, T., and I.M. Cheeseman. 2012. Chromosome- and spindle-pole-derived signals generate an intrinsic code for spindle position and orientation. *Nat. Cell Biol.* 14:311–317. http://dx.doi.org/10.1038/ncb2440

Lancaster, O.M., M. Le Berre, A. Dimitracopoulos, D. Bonazzi, E. Zlotek-Zlotkiewicz, R. Picone, T. Duke, M. Piel, and B. Baum. 2013. Mitotic rounding alters cell geometry to ensure efficient bipolar spindle formation. *Dev. Cell.* 25:270–283. http://dx.doi.org/10.1016/j.devcel.2013.03.014

Lees-Miller, J.P., D.M. Helfman, and T.A. Schroer. 1992. A vertebrate actin-related protein is a component of a multisubunit complex involved in microtubule-based vesicle motility. *Nature.* 359:244–246. http://dx.doi.org/10.1038/359244a0

Maiato, H., C.L. Rieder, and A. Khodjakov. 2004. Kinetochore-driven formation of kinetochore fibers contributes to spindle assembly during animal mitosis. *J. Cell Biol.* 167:831–840. http://dx.doi.org/10.1083/jcb.200407090

Manning, A.L., and D.A. Compton. 2007. Mechanisms of spindle-pole organization are influenced by kinetochore activity in mammalian cells. *Curr. Biol.* 17:260–265. http://dx.doi.org/10.1016/j.cub.2006.11.071

Meng, W., Y. Mushika, T. Ichii, and M. Takeichi. 2008. Anchorage of microtubule minus ends to adherens junctions regulates epithelial cell-cell contacts. *Cell.* 135:948–959. http://dx.doi.org/10.1016/j.cell.2008.09.040

Merdes, A., K. Ramyar, J.D. Vechio, and D.W. Cleveland. 1996. A complex of NuMA and cytoplasmic dynein is essential for mitotic spindle assembly. *Cell.* 87:447–458. http://dx.doi.org/10.1016/S0092-8674(00)81365-3

Merdes, A., R. Heald, K. Samejima, W.C. Earnshaw, and D.W. Cleveland. 2000. Formation of spindle poles by dynein/dynactin-dependent transport of NuMA. *J. Cell Biol.* 149:851–862. http://dx.doi.org/10.1083/jcb.149.4.851

Meunier, S., and I. Vernos. 2011. K-fibre minus ends are stabilized by a RanGTP-dependent mechanism essential for functional spindle assembly. *Nat. Cell Biol.* 13:1406–1414. http://dx.doi.org/10.1038/ncb2372

Nicklas, R.B. 1988. The forces that move chromosomes in mitosis. *Annu. Rev. Biophys. Biophys. Chem.* 17:431–449. http://dx.doi.org/10.1146/annurev.bb.17.060188.002243

Nicklas, R.B., and C.A. Staehly. 1967. Chromosome micromanipulation. I. The mechanics of chromosome attachment to the spindle. *Chromosoma.* 21:1–16. http://dx.doi.org/10.1007/BF00330544

Nicklas, R.B., D.F. Kubai, and T.S. Hays. 1982. Spindle microtubules and their mechanical associations after micromanipulation in anaphase. *J. Cell Biol.* 95:91–104. http://dx.doi.org/10.1083/jcb.95.1.91

Petry, S., A.C. Groen, K. Ishihara, T.J. Mitchison, and R.D. Vale. 2013. Branching microtubule nucleation in *Xenopus* egg extracts mediated by augmin and TPX2. *Cell.* 152:768–777. http://dx.doi.org/10.1016/j.cell.2012.12.044

Quintyne, N.J., and T.A. Schroer. 2002. Distinct cell cycle–dependent roles for dynactin and dynein at centrosomes. *J. Cell Biol.* 159:245–254. http://dx.doi.org/10.1083/jcb.200203089

Radulescu, A.E., and D.W. Cleveland. 2010. NuMA after 30 years: the matrix revisited. *Trends Cell Biol.* 20:214–222. http://dx.doi.org/10.1016/j.tcb.2010.01.003

Royle, S.J., N.A. Bright, and L. Lagnado. 2005. Clathrin is required for the function of the mitotic spindle. *Nature.* 434:1152–1157. http://dx.doi.org/10.1038/nature03502

Rusan, N.M., U.S. Tulu, C. Fagerstrom, and P. Wadsworth. 2002. Reorganization of the microtubule array in prophase/prometaphase requires cytoplasmic dynein-dependent microtubule transport. *J. Cell Biol.* 158:997–1003. http://dx.doi.org/10.1083/jcb.200204109

Saxton, W.M., D.L. Stemple, R.J. Leslie, E.D. Salmon, M. Zavortink, and J.R. McIntosh. 1984. Tubulin dynamics in cultured mammalian cells. *J. Cell Biol.* 99:2175–2186. http://dx.doi.org/10.1083/jcb.99.6.2175

Sheykhani, R., N. Baker, V. Gomez-Godinez, L.H. Liaw, J. Shah, M.W. Berns, and A. Forer. 2013. The role of actin and myosin in PtK2 spindle length changes induced by laser microbeam irradiations across the spindle. *Cytoskeleton (Hoboken).* 70:241–259. http://dx.doi.org/10.1002/cm.21104

Shimamoto, Y., Y.T. Maeda, S. Ishiwata, A.J. Libchaber, and T.M. Kapoor. 2011. Insights into the micromechanical properties of the metaphase spindle. *Cell.* 145:1062–1074. http://dx.doi.org/10.1016/j.cell.2011.05.038

Shubeita, G.T., S.L. Tran, J. Xu, M. Vershinin, S. Cermelli, S.L. Cotton, M.A. Welte, and S.P. Gross. 2008. Consequences of motor copy number on the intracellular transport of kinesin-1-driven lipid droplets. *Cell.* 135:1098–1107. http://dx.doi.org/10.1016/j.cell.2008.10.021

Silk, A.D., A.J. Holland, and D.W. Cleveland. 2009. Requirements for NuMA in maintenance and establishment of mammalian spindle poles. *J. Cell Biol.* 184:677–690. http://dx.doi.org/10.1083/jcb.200810091

Snyder, J.A., L. Armstrong, O.G. Stonington, T.P. Spurck, and J.D. Pickett-Heaps. 1991. UV-microbeam irradiations of the mitotic spindle: spindle forces and structural analysis of lesions. *Eur. J. Cell Biol.* 55:122–132.

Spurck, T.P., O.G. Stonington, J.A. Snyder, J.D. Pickett-Heaps, A. Bajer, and J. Mole-Bajer. 1990. UV microbeam irradiations of the mitotic spindle. II. Spindle fiber dynamics and force production. *J. Cell Biol.* 111:1505–1518. http://dx.doi.org/10.1083/jcb.111.4.1505

Sturgill, E.G., and R. Ohi. 2013. Kinesin-12 differentially affects spindle assembly depending on its microtubule substrate. *Curr. Biol.* 23:1280–1290. http://dx.doi.org/10.1016/j.cub.2013.05.043

Tulu, U.S., N.M. Rusan, and P. Wadsworth. 2003. Peripheral, non-centrosome-associated microtubules contribute to spindle formation in centrosome-containing cells. *Curr. Biol.* 13:1894–1899. http://dx.doi.org/10.1016/j.cub.2003.10.002

Verde, F., J.M. Berrez, C. Antony, and E. Karsenti. 1991. Taxol-induced microtubule asters in mitotic extracts of *Xenopus* eggs: requirement for phosphorylated factors and cytoplasmic dynein. *J. Cell Biol.* 112:1177–1187. http://dx.doi.org/10.1083/jcb.112.6.1177

Vladimirou, E., N. Mchedlishvili, I. Gasic, J.W. Armond, C.P. Samora, P. Meraldi, and A.D. McAinsh. 2013. Nonautonomous movement of chromosomes in mitosis. *Dev. Cell.* 27:60–71. http://dx.doi.org/10.1016/j.devcel.2013.08.004

Yang, G., L.A. Cameron, P.S. Maddox, E.D. Salmon, and G. Danuser. 2008. Regional variation of microtubule flux reveals microtubule organization in the metaphase meiotic spindle. *J. Cell Biol.* 182:631–639. http://dx.doi.org/10.1083/jcb.200801105

Zheng, Y., M.L. Wong, B. Alberts, and T. Mitchison. 1995. Nucleation of microtubule assembly by a γ-tubulin-containing ring complex. *Nature.* 378:578–583. http://dx.doi.org/10.1038/378578a0